5-2010

Linear-Nonlinear Interaction and Passive Intermodulation Distortion

Justin Henrie
Purdue University, jhenrie@purdue.edu

Andrew Christianson
Purdue University, christaj@purdue.edu

William J. Chappell
School of Electrical and Computer Engineering, Birck Nanotechnology Center, Purdue University, chappell@purdue.edu

Linear–Nonlinear Interaction and Passive Intermodulation Distortion

Justin J. Henrie, *Student Member, IEEE*, Andrew J. Christianson, *Student Member, IEEE*, and William J. Chappell, *Member, IEEE*

***Abstract*—This paper describes several consequences of a linear–nonlinear interaction that was recently found to be of importance in microwave circuits that produce passive intermodulation (PIM) distortion. This paper briefly discusses how this linear–nonlinear interaction operates in an example system. It then discusses how an understanding of the linear–nonlinear interaction allows us to distinguish between different types of nonlinearities from the power dependence of the third-order intermodulation distortion product. Next, an example uses a multiphysics simulator to demonstrate that electrothermal nonlinearities behave as expected from the linear–nonlinear interaction model. Lastly, it illustrates how simple nonlinear models characterized with one circuit can accurately predict distortion levels when the nonlinearity is placed within a very different circuit, showing that knowledge of the interaction gives the ability to accurately predict the behavior of PIM-producing components in a variety of circuits such as resonators, filters, and matching networks.**

***Index Terms*—Communication system nonlinearities, interchannel interference, nonlinear circuits, nonlinear distortion, passive intermodulation (PIM).**

I. Introduction

ATTEMPTS TO construct analytical models of nonlinearity usually begin with a simple truncated power series or Volterra series expansion [1], [2]. However, for many passive systems such as coaxial connectors and unsoldered waveguide flanges, a third- or fifth-order nonlinear model is not sufficient to characterize the nonlinear response of the entire system. Very high-order expressions are required, which are difficult to tie to a physical or intuitive understanding of the nonlinearity. For example, the power dependence of passive intermodulation (PIM) producing nonlinearities in high-powered components such as coaxial connectors, filters, antennas, and transmission lines is difficult to model by analytical methods, although several useful studies have shed light on other aspects of these systems [3], [4]. Modeling of the power dependence of the distortion products of these nonlinearities has thus far been hampered by the apparent multiorder nature of PIM in microwave networks [5]–[9].

We showed in [10] that the intermodulation distortion (IM) of low-impedance passive components such as coaxial connectors is strongly influenced by an interaction between the passive nonlinearity and its surrounding impedances. Such linear–nonlinear interactions have been extensively studied as relating to active devices such as amplifiers and mixers [11]–[14]. However, the effects of the load and other impedances as pertaining to PIM production have until now been restricted mainly to linear reflections, and have not probed the interaction between these impedances and the nonlinearity itself. An example of this is [15] and [16], useful studies that account for the reflectivities around the nonlinearity. However, these studies specifically preclude linear–nonlinear interaction by considering the impedance of the nonlinearity to "be negligible compared with the source and load impedances" [15]. Due to this, important parameters such as the power dependence of system PIM cannot be modeled correctly by such studies.

The implications of linear–nonlinear interaction are important in understanding and modeling the low-impedance nonlinearities of the passive components that normally contribute to PIM distortion. This paper provides a treatment of some of the effects of this interaction and its implications in understanding and modeling microwave components and systems that produce PIM. First, we describe the linear–nonlinear interaction from an RF perspective as opposed to the more general description given in [10]. We then show that knowledge of this linear–nonlinear interaction in microwave systems gives an important indication as to the nature of the physical mechanism of passive nonlinearity, which for many components is still an unknown [4], [9], [17]. Finally, we show that the knowledge of this interaction allows nonlinear components to be characterized independently of their surrounding circuit. This enables the prediction of PIM production in complicated circuits based on the measurement of PIM sources in simple circuits, such as that shown in Fig. 1.

II. Description of Linear–Nonlinear Interaction

In addition to the description in [10], another perspective on the interaction between R_L and R_{NL} in the circuit of Fig. 1 could be helpful in developing a physical understanding. Fig. 1 depicts a circuit frequently tested by our PIM analysis system, which is the serial combination of a PIM source (a subminiature A (SMA) connector) with a 50-Ω load. In this network, the PIM of the nonlinearity is at least 20 dB higher than all other PIM sources, allowing us to treat all other components as being linear. We noted in [10] that the distribution of voltage between

Manuscript received March 26, 2009; revised September 25, 2009. First published April 12, 2010; current version published May 12, 2010. This work was supported in part by the U.S. Army Research Office as a Multi-disciplinary University Research Initiative on Standoff Inverse Analysis and Manipulation of Electronic Systems under Grant W911NF-05-1-0337.

The authors are with the Electrical and Computer Engineering Department and the Birck Nanotechnology Center, Purdue University, West Lafayette, IN 47907 USA (e-mail: jhenrie@purdue.edu; christaj@purdu.edu; chappell@purdue.edu).

Color versions of one or more of the figures in this paper are available online at http://ieeexplore.ieee.org.

Digital Object Identifier 10.1109/TMTT.2010.2045527

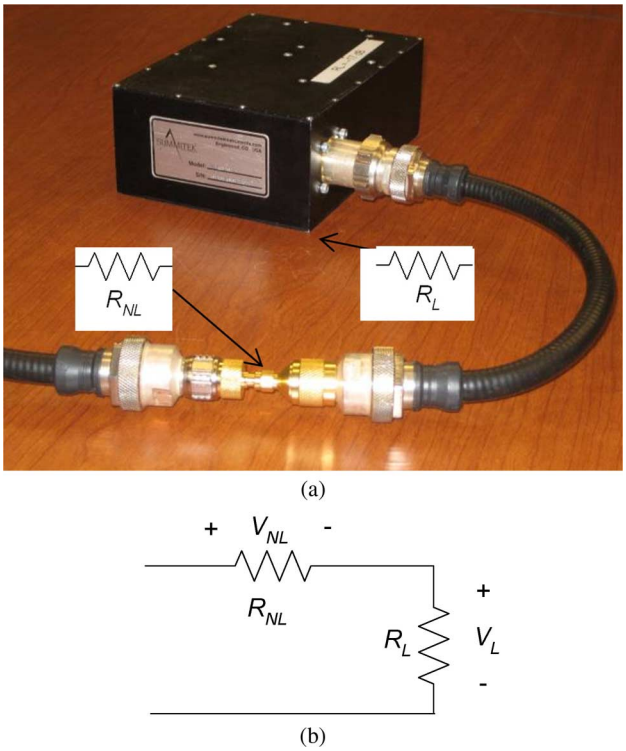

Fig. 1. (a) Photograph of the measurement configuration of the SMA connector discussed in this paper. Here, the SMA connection in the foreground is connected in series with a 50-Ω low-PIM dummy load. Shown in (b) is a simplified circuit model, consisting of a nonlinear resistor (the SMA connector) in series with a 50-Ω resistor (the dummy load) used to describe this measurement setup.

the two resistors shown in Fig. 1(b) is not constant, but in fact changes continuously with V_g. This is a result of the nonlinear series resistance of the SMA connector R_{NL}. An expression for the voltage dropped across the nonlinear resistor can be obtained by solving [10, eq. (2)] for the voltage drop across the nonlinear resistor, the bracketed quantity $V_{NL} = [V_g - I(V_g)R_L]$. This solution yields the expression for this voltage

$$V_{NL} = \frac{\left(\frac{2}{3}\right)^{1/3} a_1}{\left(-9a_3^2 I(V_g) + \sqrt{3}\sqrt{4a_1^3 a_3^3 + 27a_3^4 I(V_g)^2}\right)^{1/3}} - \frac{\left(-9a_3^2 I(V_g) + \sqrt{3}\sqrt{4a_1^3 a_3^3 + 27a_3^4 I(V_g)^2}\right)^{1/3}}{2^{1/3}3^{2/3}a_3} \quad (1)$$

where $I(V_g)$ is given by [10, eq. (3)], and a_1 and a_3 are the linear and cubic coefficients to the resistor's *I–V* curve, as given in [10, eq. (1)], repeated here for convenience

$$I(V_{NL}) = a_1 V_{NL} + a_3 V_{NL}^3. \quad (2)$$

By multiplying (1) and $I(V_g)$ (see [10, eq. (3)]), we can derive the total power across the resistor as a function of the input voltage or power. This product is plotted for a two-tone excitation in Fig. 2(a), where the power absorbed by the nonlinear resistor (dashed line), is compared to the third-order intermodulation (IM3) power output by the resistor (solid line).

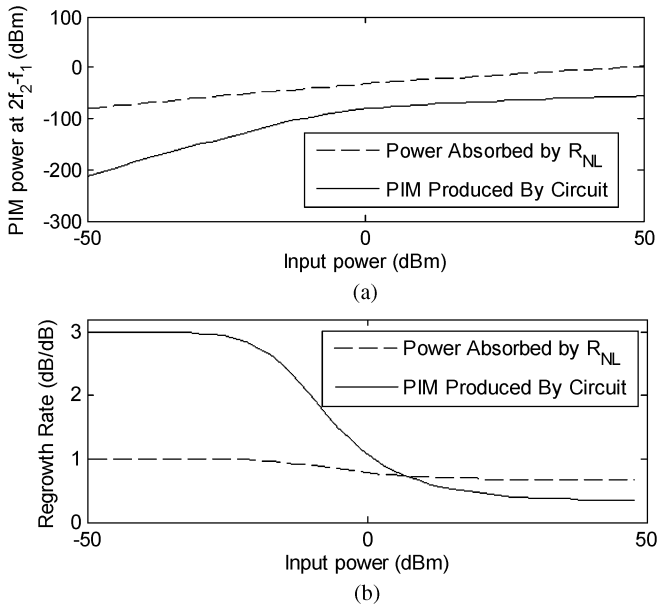

Fig. 2. (a) Power absorbed by the nonlinear resistor (solid line) and the intermodulation power output by the circuit (dashed line) in Fig. 1. (b) First derivative of the curves shown in (a).

Fig. 2(b) shows the slope of the two curves shown in Fig. 2(a). We see first that at low input power when the PIM regrowth slope is 3 dB/dB, the power dropped across the resistor is directly proportional to the input power. At roughly −10-dBm input power, the slope of the PIM curve begins to drop, and we see a corresponding drop in the slope of the linear input power dropped across the resistor. This diminution in the proportion of input power absorbed by the nonlinear resistor is a consequence of the nonlinear resistance R_{NL} becoming less resistive at higher voltage. The result is a drop in the proportion of the total voltage over the nonlinear resistor, caused by the diminishing magnitude of R_{NL} in (2). This lessening in the proportion of V_g that is dropped across the nonlinear resistor is of course accompanied by a larger portion of V_g being dropped across the completely linear R_L. This 'shift' of power from the nonlinear to linear resistances of the system is the direct cause of the drop in the regrowth rate of its PIM output: as a lower proportion of the input voltage is absorbed by the nonlinear resistor, its nonlinearity in general and PIM output in particular become similarly diminished.

It is instructive to note that the lessening in slope of the IM power produced by the resistor and the linear power absorbed by the resistor occur simultaneously. Before this point, the voltage division between the linear and nonlinear resistors is essentially static. Due to this, the power dropped across R_{NL} is proportional to V_g and its IM response is essentially cubic, meaning that the IM power is proportional to the cube of the input power. This is evinced by the 3-dB/dB regrowth rate of IM with input power up to this power level. After this, the fraction of the total power absorbed by the nonlinear resistor diminishes. This causes a corresponding diminution in the IM power produced. This signals the onset of linear–nonlinear interaction, which also produces the higher order behavior of the circuit, as shown in [10].

III. Decreasing- and Increasing-Resistance Nonlinearities

A fundamental characteristic of the nonlinear resistor's behavior is determined by the sign of the coefficient a_3 in its *I–V* expression (2). Many physical nonlinearities can be modeled as memoryless monotonic resistive nonlinearities whose resistance either increases or decreases with increasing voltage [5], [18]. Both types of resistive nonlinearity occur in nature, and the power dependencies of both types of nonlinearity in circuits are distinct from one another. This section will describe briefly the salient differences in the power dependencies of both types of nonlinearity. In particular, it is found that for the series configuration we investigate here [see Fig. 1(b)], IM3 products of decreasing-resistance nonlinearities can have a regrowth rate of $\leq$3 dB/dB, while those of increasing-resistance nonlinearities have a regrowth rate of $\geq$3 dB/dB. This allows the two different types of nonlinearity to be differentiated from each other in a swept-power measurement.

A. Decreasing-Resistance Nonlinearities

The name "decreasing-resistance nonlinearities" is given because they tend toward a short-circuit: resistance decreases with increasing applied voltage. The "forward-biased" side of a diode's *I–V* curve is an example of this type of nonlinearity, which is a concave-up function with increasing voltage magnitude. More examples could include corona discharge and dielectric breakdown [19], and electron tunneling across a potential barrier where the imposed voltage lowers the energy barrier [20]. The simple third-order model for these nonlinearities would have positive a_3 in (2).

When nonlinear impedances are combined with the series impedance of an external circuit, the result is a division of the source voltage across all the resistances; such as that given for our example circuit by [10, eq. (4)]. For decreasing-resistance nonlinearities, the resistance of the element decreases with increasing voltage, so the result of the voltage division is that successively less of the driving voltage of a circuit is dropped across the nonlinearity as the driving voltage increases. The other impedances in the circuit will then dominate the nonlinear element's contribution to the circuit's behavior at higher driving voltages. This makes the circuit less nonlinear at higher input voltages than one might expect from its low-voltage operation. This can be seen in Fig. 2, where the reduction in the regrowth rate of the IM product substantially reduces its value at high input powers from what would be expected had its regrowth rate remained constant at 3 dB/dB. Many passive microwave devices, such as nickel-containing components and many resistive loads, which generate the PIM distortion commonly encountered in real systems, display this characteristic [7], [8], [21], [22].

B. Increasing-Resistance Nonlinearities

Increasing-resistance nonlinearities are so named because their resistance increases with increasing voltage—tending toward an open circuit. These nonlinearities display a concave-down *I–V* curve. Nonlinearities of this kind could include the saturation velocity of carriers in semiconductors [23] or the electrothermal effect, where Joule heating in a metal causes an increase in the metal's temperature, and hence, its resistivity [4], [24]. The third-order model for these types of resistive nonlinearities has a negative value for a_3 in (2). In a swept-power two-tone test, increasing-resistance nonlinearities display a fundamentally different behavior than decreasing-resistance nonlinearities. Let us consider again the example circuit given in Fig. 1(b). If R_{NL} is an increasing-resistance nonlinearity, the voltage division between R_{NL} and R_L given by [10, eq. (4)] is no longer a decreasing function with voltage, but in fact, increases as V_g increases. Therefore, the proportion of total power absorbed by R_{NL} increases as input power increases, and by the same reasoning we followed in Section II, we expect the IM regrowth rate to increase as input power increases. This expectation is confirmed by simulation: the actual behavior of our example circuit where R_{NL} is an increasing-resistance nonlinearity is shown in Fig. 3. Here the value of a_3 is set to -10^2, and a_1 is 10.

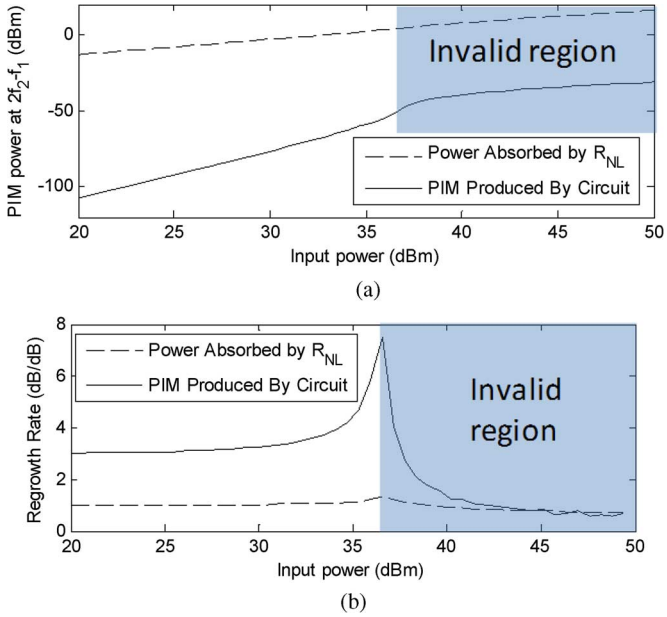

Fig. 3. (a) Input power absorbed by R_{NL} (dotted line) and the third-order IM power produced by the example circuit (solid line) for $a_3 < 0$. (b) Derivatives of the curves shown in (a).

As in Fig. 2, we plot the power in the third-order IM product (solid line), as well as the power absorbed by the nonlinear resistor (dotted line) in Fig. 3(a), while the slopes of these lines are displayed in Fig. 3(b). Like the decreasing-resistance nonlinearity, for low input powers, the IM product's power increases proportional to the cube of the input power; the circuit's behavior is essentially third order. At about 30 dBm input power, we then see the regrowth rate begin to rise. This is due to the increasing average impedance of R_{NL} as input power increases, which results in an increase in the proportion of total power absorbed by R_{NL} and a corresponding increase in its IM output. However, this augmentation of regrowth rate continues only until about 38-dBm input power, when the slope abruptly falls to a low value and undergoes rather "noisy" behavior. Actually, the plotted behavior past the maximum point on Fig. 3 is invalid, as the representation of the nonlinear resistor at this point

becomes nonphysical. To see why this is, we examine the resistance of R_{NL} with our stated value of $a_3 = -10^2$. Since the two terms of (2) are opposite in sign for negative a_3, the current initially increases in the region where the linear term dominates, then decreases through zero and becomes negative for higher input voltages. The voltage at which the current through the resistor vanishes is given by

$$V_{\text{zero}} = \frac{\sqrt{a_1}}{\sqrt{|a_3|}}. \tag{3}$$

At this zero point, the resistance of R_{NL} becomes infinite and all the voltage in the system is dropped across it. Beyond this point, the resistance of R_{NL} becomes negative. This is obviously a nonrealistic situation for the passive nonlinear components we examine in this example. Our model also breaks down past this point, as the solution we chose for positive values of R_{NL} (see [10, eq. (4)]) becomes complex when R_{NL} goes negative.

We verify this regrowth rate augmentation property of increasing-resistance nonlinearities with a coupled-physics simulation in Section III-C.

C. Example of an Increasing-Resistance Nonlinearity: Microscopic Electrical Contact Undergoing Electrothermal Nonlinearity

As an example of an increasing-resistance nonlinearity, we use a coupled-physics finite-element package to simulate one of the nonlinearities that is likely to occur in the unsoldered metal–metal contacts of coaxial connectors—electrothermal nonlinearity at the microscopic contact asperities, or "a-spots" [25]. The resistance of all bulk metals increases with increasing temperatures [26] (this in contrast to semiconductors, whose resistance initially decreases with increasing temperature). The electrothermal effect can cause *I–V* nonlinearity because Joule heating in the metal is more pronounced at higher current levels, causing the resistance of the metal to increase at higher voltages. The contribution of this nonlinearity to PIM in different components has been studied in [4], [24], and [27].

We examine the behavior of this system's third-order PIM product under a two-tone test. It is found that the greater-than cubic regrowth rate of PIM, as predicted by our model (shown in Fig. 3), is manifested in this system.

As in most electrical connectors, one of the prime objectives in the design of a coaxial connector is to provide an electrical connection with as low a resistance as possible. Contact resistances are encountered at unsoldered contacts because the actual contact area is always rather small due to the fact that on the microscale, there is significant roughness to any metal surface. As a result, when two metal contacts are brought together, actual electrical contact is only achieved at discrete spots where asperities on either surface coincide sufficiently to make contact. In order to investigate the PIM distortion produced by the unsoldered contacts in coaxial connectors, we created a finite-element model of one of these "a-spot" regions in COMSOL, a time-domain coupled-physics simulation package. The small size and relatively low-frequency operation (around 500 MHz) of the

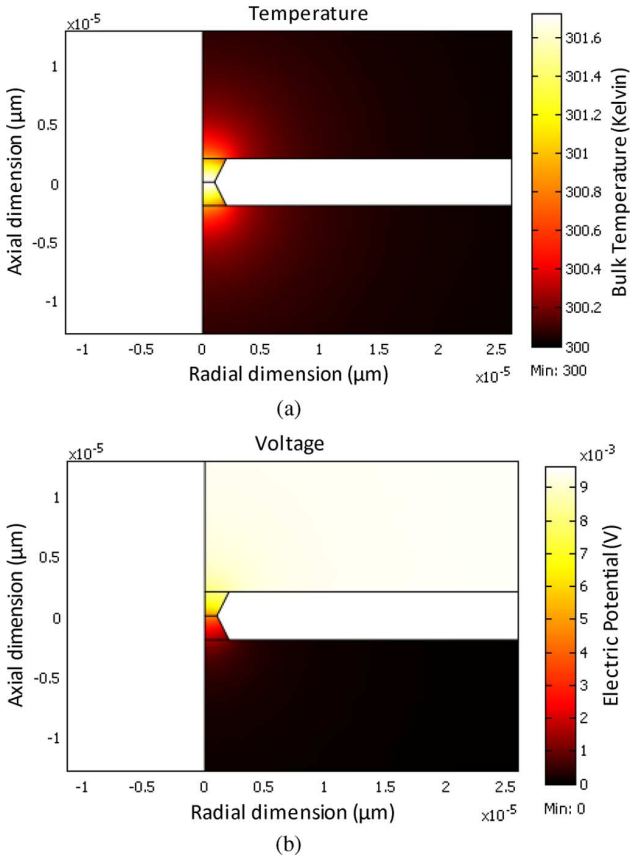

Fig. 4. Axially-symmetric cross section of an "a-spot" of a copper-copper metallic contact simulation in COMSOL Multiphysics, where both the electrical and thermal governing relationships are solved simultaneously in the time domain. Current flow through the a-spot induces: (a) a temperature rise in the restriction due to Joule heating, which affects the voltage drop of the a-spot (b) through the temperature-dependent change in resistance of the copper metal.

system allow us to use COMSOL's ac/dc application mode, which solves the quasi-static electrical conduction equation

$$-\nabla \cdot \frac{\partial(\varepsilon \nabla V)}{\partial t} - \nabla \cdot (\sigma \nabla V - J^e) = Q_j \tag{4}$$

where V is electric potential, ε is the permittivity of insulators, σ is the temperature-dependent conductivity of conductors, J^e is the electric current density, and Q_j is volumetric heat flux produced by conductor losses (Joule heating). This loss mechanism becomes the heat source to a thermal cosimulation, governed by the thermal diffusion equation

$$\rho C_p \frac{\partial T}{\partial t} - \nabla \cdot (k \nabla T) = Q_j \tag{5}$$

where ρ is material density, C_p is thermal capacity, and k is a temperature-dependent thermal conductivity term.

In this model, both the electrical conduction equation and the thermal diffusion equation are solved simultaneously in order to properly account for the interrelationship between the voltage drop across the junction and the junction's temperature. Representative plots of both the voltage drop across the junction and the temperature of the junction are shown in Fig. 4. In this figure, the left edge of the structure is an axial symmetry plane, around which the displayed cross section is rotated to yield the 3-D a-spot model. For the model shown in Fig. 4, the a-spot

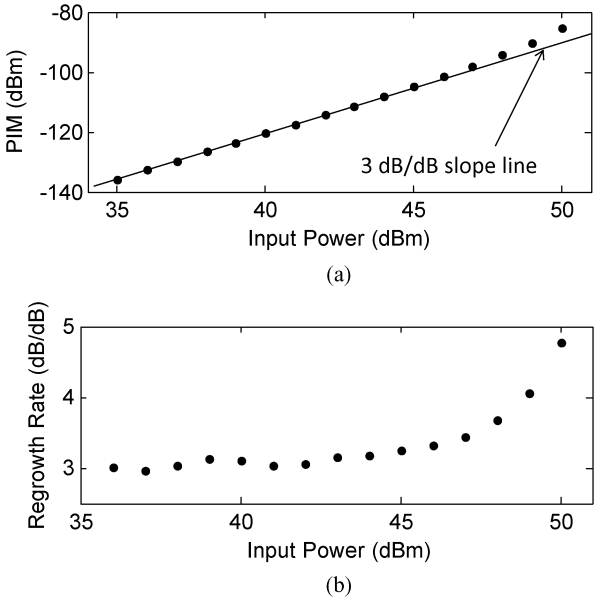

Fig. 5. Plots of: (a) the power of the third-order PIM distortion produced by the a-spot contact shown in Fig. 4 under a two-tone test. (b) Regrowth rate of the nonlinearity. We note that the regrowth rate of the system increases from an initial cubic dependence, as predicted by the interaction model.

restriction has a diameter of 4 μm at the top and bottom electrodes (the upper and lower rectangular regions), narrowing to a minimum diameter of 2 μm in its center. The top and bottom electrodes, representing the large-scale faces of the metal–metal contact, are made large in comparison to the constriction. Due to this, their electrical dissipation can be neglected and their faces not adjacent to the a-spot can be set to a constant temperature. The standard material parameters of bulk copper metal are used in this simulation. The electrical properties include a temperature-dependent electrical conductivity $\sigma(T)$ given by

$$\sigma(T) = \frac{1}{\rho_0 + \alpha(T - T_0)} \frac{10^9 S}{m} \tag{6}$$

where $\rho_0 = 16.78$ n$\Omega \cdot$ m is the room-temperature resistivity ($T_0 = 300$ K), $\propto = .004041$ n$\Omega \cdot$m/K is the temperature coefficient of resistance of copper, and T is the temperature in Kelvin [28].

The thermal properties include a density of 8700 kg/m^3, a heat capacity of 385 J/kg $\cdot$ K, and a temperature-dependent thermal conductivity k determined by the Wiedemann–Franz Law [18]

$$k = \frac{LT}{\sigma(T)} \text{W/m} \cdot \text{K} \tag{7}$$

where $L = 2.45 \cdot 10^{-8}$ V^{2}K^{-2} is the Lorentz constant and $\sigma(T)$ is given by (6).

The simulated a-spot was subjected to a two-tone test similar to that generated by our measurement system; the results are displayed in Fig. 5. We see that the IM3 signal behaves as the interaction model suggests—increasing with the cube of the input power initially, and then increasing more rapidly with increasing power as the thermal change in resistance becomes significant. Interestingly, just as [10, eq. (3)] predicts nonphysical behavior soon after this augmentation in regrowth rate, so too does the a-spot model. The multiphysics simulation shows rapidly increasing temperature at the a-spot at input powers inducing greater than cubic power dependence. The temperature rise becomes unbounded and the numerical simulation diverges. This investigation in the PIM distortion produced by the electrothermal nonlinearity at the "a-spot" contact surfaces of coaxial connectors confirms the $\geq$3-dB/dB regrowth rate dependence of this type of increasing-resistance nonlinearity, as can be predicted by considering the interaction of nonlinearities of this type with series linear impedances. Perhaps more interesting, the characteristic $\geq$3-dB/dB dependency shows that this electrothermal nonlinearity is not the dominant source of nonlinearity that is measured in SMA connectors, as discussed in Section III-D.

D. Comparing Increasing-Resistance and Decreasing-Resistance Nonlinearities

One of the utilities of the observations in this section is the ability to distinguish between the two types of nonlinearity by their different behaviors in a two-tone test. If the regrowth rate of an IM product diminishes with increasing input power (such as in Fig. 2), we can infer that the physical process causing the nonlinearity in the circuit is a decreasing-resistance nonlinearity such as is typified by a forward-biased diode. As stated before, nickel-containing wireless components [7] and many resistive loads [22] display this characteristic, yielding PIM-versus-input power relationships, such as that depicted in Fig. 2 or Fig. 6, where the regrowth rate of the PIM is $\leq$3 dB/dB. This decreasing power dependence with increasing input power has also been observed for the PIM generated by unsoldered metal–metal contacts [29], including the unsoldered metal–metal connections of aluminum waveguide flanges [21]. Due to this, we can infer that the dominant passive nonlinearity in these components is a decreasing-resistance and not an increasing-resistance nonlinearity, such as the electrothermal effect. Conversely, if the regrowth rate rises with increasing input power (such as in Figs. 3 or 5), this gives evidence that the underlying physical nonlinearity is an increasing-resistance process.

IV. Extraction of Model Parameters for Prediction of IM Behavior in Arbitrary Circuit Topologies

An important capability conferred by the awareness of this linear–nonlinear interaction is the ability to fit simple *I–V* expressions such as (2) to passive nonlinear components in one circuit, and then use these models in complex circuits to accurately predict the nonlinear behavior of other circuits that incorporate these nonlinearities. We demonstrate this by using the simple *I–V* expression of an SMA connection that fits the data from a two-tone test in the configuration shown in Fig. 1 to predict the nonlinear response of the SMA connector in a microstrip resonator.

For the through-line measurement, we placed an SMA connector in series with our measurement system's 50-Ω load, as described in [6]. One slight modification to the system is that a microwave attenuator is employed when the value of the PIM output of the system is over -70 dBm to avoid saturation of the receive circuitry. The power in the carrier tones was swept from

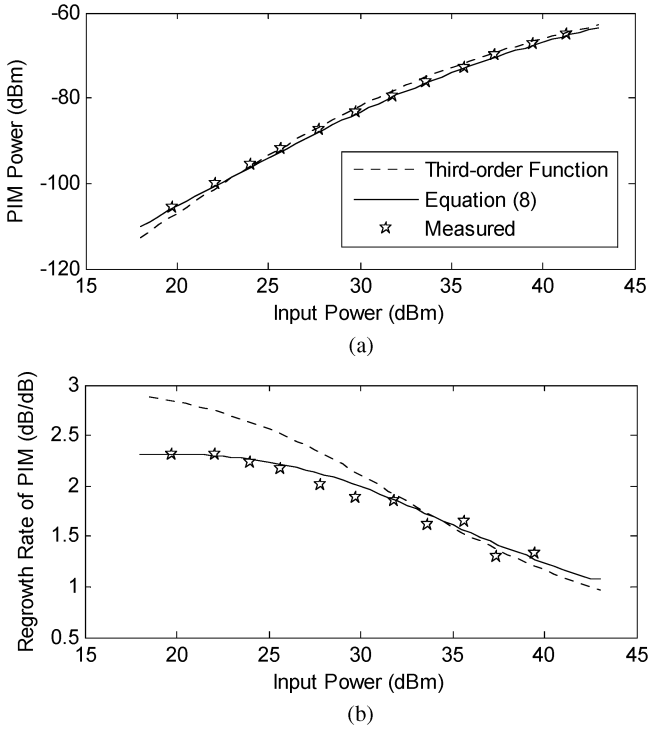

Fig. 6. Simulated (lines) and measured (stars): (a) power dependence of the IM of an SMA connection in a two-tone test along with (b) the first derivative of each curve. The dotted line depicts optimal modeling obtained with a purely third-order component nonlinearity (2), while the solid line shows the improvement obtained by adding a quasi-quadratic term to the component nonlinearity (8).

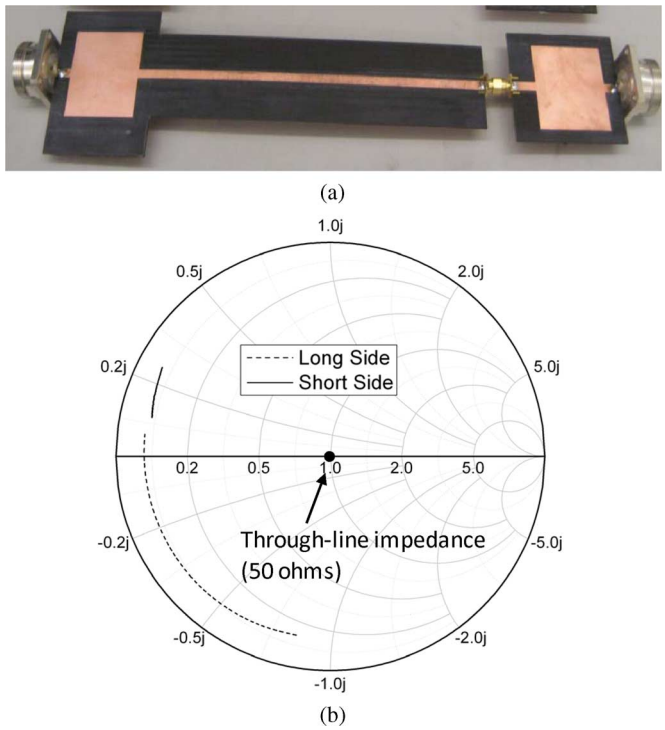

Fig. 7. (a) Photograph of the microstrip resonator whose PIM was predicted by representing the SMA *I–V* curve with (8), whose coefficients were fit in a previous experiment with a circuit of a different topology which presented a 50-Ω impedance to the SMA connector. (b) Smith Chart plots of the input impedance seen at the SMA connection when looking through the longer side of the resonator (lower line) or the shorter side of the resonator (upper line) in the frequency range of 400–500 MHz.

20 to 42 dBm, and an interaction model of the type shown in Fig. 1(b) was fit to the data using both (2) and also a slightly refined *I–V* function, which includes the addition of a nonrectifying quadratic term

$$I(V_{NL}) = a_1 V_{NL} + \frac{a_2 V_{NL}^3}{|V_{NL}|} + a_3 V_{NL}^3. \tag{8}$$

The second term in (8) is "quasi-quadratic" in that (in isolation) the IM products produced by this term have a 2-dB/dB regrowth rate. However, it is an odd function with voltage, and therefore, characterized by a purely odd-ordered power series. Its inclusion in the *I–V* description of R_{NL} helps to match the low-power regrowth rate better to experiment.

Both the measurement data and the fit of the two models are shown in Fig. 6. We next used the values of the a_1, a_2, and a_3 coefficients from (8) that were used in producing the curves of Fig. 6 to predict the PIM of a microstrip resonator containing a similar SMA connector.

This resonator is displayed in Fig. 7(a). For this experiment, we placed the PIM source (an SMA connection) into a microwave resonator, which was formed by placing a length of 50-Ω microstrip between two low-impedance sections of transmission line. This length of 50-Ω line contains the SMA connection. This resonator was made on Rogers 5880 1.575-mm-thick substrate. The two low-impedance capacitive sections are squares of 45.8 mm to a side, and are separated by 258 mm of 50-Ω transmission line. The resonator has its first resonant frequency at 466.5 MHz (midway between the two carrier frequencies of the two-tone test) with a quality factor of approximately 14. To verify that the measured IM of the network was dominated by the embedded SMA connection, a control resonator without an SMA connection was milled from a single substrate (with no SMA connection within the resonator) and measured in the same two-tone test used to evaluate the resonator, which included the SMA connection. This control network produced −97 dBm of PIM under a maximum-power (43 dBm per carrier) two-tone test; almost 40 dB lower than that produced by the resonator with the SMA connection, establishing that the IM measured from the resonator incorporating the SMA connection is dominated by the PIM response of the SMA connection and not the microstrip resonator itself.

The impedances seen by the SMA nonlinearity in this circuit are much different than the frequency-independent 50-Ω impedance of the circuit of Fig. 1. These impedances are plotted in Fig. 7(b) over the frequency range of 400–500 MHz, which is the approximate range of nonlinear operation in this two-tone test, whose input tones were set at 463 and 468 MHz.

The measurements and model predictions for the PIM output of the network shown in Fig. 7(a) is graphed in Fig. 8. In this plot, the power in each carrier tone is reported on the horizontal axis, as with Fig. 6. The increase in PIM output of the SMA connector over that shown in Fig. 6 is shown on the vertical axis.

The result of the different impedances seen by the SMA nonlinearity was a dramatic increase of the PIM output of the SMA

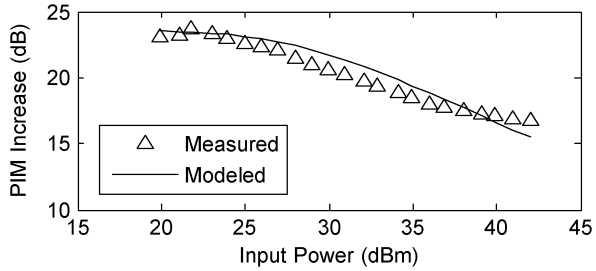

Fig. 8. Measured (triangles) versus simulated (line) behavior of the increase of the IM produced by an SMA connector within a resonator over that of the same connector within the 50-Ω through line, as shown in Fig. 6. The same coefficients a_1, a_2, and a_3 for R_{NL} (8) were used in both tests.

connector in the microwave resonator as compared to that produced by the SMA connector in the 50-Ω circuit shown in Fig. 1. However, the component *I–V* nonlinearity (8), which was fit for the SMA connector in the 50-Ω network of Fig. 1, accurately predicted the 20+-dB PIM enhancement due to the resonator. This enhancement is because the higher currents present at the SMA connector's location within the resonator excite a higher level of PIM from this current-dependent nonlinearity [30]. Another interesting feature shown in Fig. 8 is that the regrowth rate of the IM produced by the SMA connector is lower for the in-resonator case, as shown by the smaller factor PIM enhancement over the through-line circuit as input power increases. The impedances "seen" by the SMA nonlinearity in the resonator interact differently than in the through-line case we derived analytically in [10]. Thus, by placing the SMA connector within the resonator, we change the external impedances with which it interacts without changing the *I–V* description of the nonlinearity itself. The fact that the same *I–V* description (8) is able to predict the IM behavior of the SMA connection in and out of the resonator shows that the nonlinearity of the SMA connector is independent of the external circuit. Thus, once the parameters for component descriptions such as (8) are ascertained, they can be used to predict the PIM production of the components they describe in different circuit topologies.

V. Future Work

This paper has only explored the interaction of memoryless resistive nonlinear networks in series connection with an exterior circuit. Although interactions of this type have been successful in predicting the behavior of coaxial connectors, it is likely that other aspects of passive nonlinear components would not be adequately described by the models we have discussed in this work. For example, the time constant of a nonlinearity, as studied by Wilkerson *et al.* [24], [27] could not be described by the purely resistive (and therefore, memoryless) nonlinear networks studied here. The models developed in [24] and [27], however, would likely be very successful at predicting the overall PIM response of systems containing the types of nonlinearity studied therein after accounting for the interaction effect studied in this paper.

In this paper, we have also not analyzed systems where nonlinearity is in a parallel, rather than series connection, with the external circuit. An example of such a nonlinearity could be the nonlinear permittivity of the dielectric material of a transmission line. Such dielectric nonlinearities are common in the optical regime [31] and parallel nonlinearities have been found in microwave systems as well [30].

Most important will be the impact of this study on "root-principles" studies of PIM distortion, which aim to predict component PIM as a result of actual physical nonlinear processes. Such studies have been undertaken in the past (e.g. [4], [9], and [17]), but no theoretical study to our knowledge has yet predicted experimentally measured PIM. It is hoped that future studies of PIM from a root-principles perspective will be aided by this work's identification of this interaction and its consequent clarification of the description of the nonlinear component itself.

VI. Conclusion

This paper describes several consequences of a linear–nonlinear interaction that was recently found to be of importance in microwave circuits that produce PIM distortion [10]. This paper briefly discusses how this linear–nonlinear interaction operates in an example system. It then discusses how an understanding of the linear–nonlinear interaction allows us to distinguish between different types of nonlinearities from the power dependence of the third-order IM product. Next, an example uses a multiphysics simulator to demonstrate that electrothermal nonlinearities behave as expected from the linear–nonlinear interaction model. Lastly, it illustrates how simple nonlinear models characterized with one circuit can accurately predict distortion levels when the nonlinearity is placed within a very different circuit, showing that knowledge of the interaction gives the ability to accurately predict the behavior of PIM-producing components in a variety of circuits such as resonators, filters, and matching networks.

References

[1] J. C. Pedro and N. B. Carvalho, *Intermodulation Distortion in Microwave and Wireless Circuits*. Boston, MA: Artech House, 2003.
[2] D. D. Weiner and J. F. Spina, *Sinusoidal Analysis and Modeling of Weakly Nonlinear Circuits*, 1st ed. New York: Van Nostrand, 1980.
[3] J. Mateu, C. Collado, N. Orloff, J. C. Booth, E. Rocas, A. Padilla, and J. M. O Callaghan, "Third-order intermodulation distortion and harmonic generation in mismatched weakly nonlinear transmission lines," *IEEE Trans. Microw. Theory Tech.*, vol. 57, no. 1, pp. 10–18, Jan. 2009.
[4] J. Wilcox and P. Molmud, "Thermal heating contribution to intermodulation fields in coaxial waveguides," *IEEE Trans. Commun.*, vol. COM-24, no. 2, pp. 238–243, Feb. 1976.
[5] P. Bolli, S. Selleri, and G. Pelosi, "Passive intermodulation on large reflector antennas," *IEEE Antennas Propag. Mag.*, vol. 44, pp. 13–20, Oct. 2002.
[6] A. J. Christianson, J. J. Henrie, and W. J. Chappell, "Higher order intermodulation product measurement of passive components," *IEEE Trans. Microw. Theory Tech.*, vol. 56, no. 7, pp. 1729–1736, Jul. 2008.
[7] J. Henrie, A. Christianson, and W. J. Chappell, "Prediction of passive intermodulation from coaxial connectors in microwave networks," *IEEE Trans. Microw. Theory Tech.*, vol. 56, no. 1, pp. 209–216, Jan. 2008.
[8] P. L. Lui, "Passive intermodulation interference in communication systems," *Electron. Commun. Eng. J.*, vol. 2, pp. 109–118, Jun. 1990.
[9] C. Vicente and H. L. Hartnagel, "Passive-intermodulation analysis between rough rectangular waveguide flanges," *IEEE Trans. Microw. Theory Tech.*, vol. 53, no. 8, pp. 2515–2525, Aug. 2005.
[10] J. Henrie, A. Christianson, and W. J. Chappell, "Linear–nonlinear interaction's effect on the power dependence of nonlinear distortion products," *Appl. Phys. Lett.*, vol. 94, Mar. 2009, Art. ID 114101.
[11] N. Borges de Carvalho and J. C. Pedro, "A comprehensive explanation of distortion sideband asymmetries," *IEEE Trans. Microw. Theory Tech.*, vol. 50, no. 9, pp. 2090–2101, Sep. 2002.

[12] J. Brinkhoff and A. E. Parker, "Effect of baseband impedance on FET intermodulation," *IEEE Trans. Microw. Theory Tech.*, vol. 51, no. 3, pp. 1045–1051, Mar. 2003.
[13] S. C. Cripps, "RF power amplifiers for wireless communications," *IEEE Microw. Mag.*, vol. 1, pp. 64–64, 2000.
[14] S. A. Maas, *Nonlinear Microwave and RF Circuits*. Norwood, MA: Artech House, 2003.
[15] S. Hienonen, "Effect of load impedance on passive intermodulation measurements," *Electron. Lett.*, vol. 40, pp. 245–7, Feb. 2004.
[16] D. E. Zelenchuk, A. P. Shitvov, A. G. Schuchinsky, and V. F. Fusco, "Passive intermodulation in finite lengths of printed microstrip lines," *IEEE Trans. Microw. Theory Tech.*, vol. 56, no. 11, pp. 2426–2434, Nov. 2008.
[17] J. Russer, A. Ramachandran, A. Cangellaris, and P. Russer, "Phenomenological modeling of passive intermodulation (PIM) due to electron tunneling at metallic contacts," in *IEEE MTT-S Int. Microw. Symp. Dig.*, 2006, pp. 1129–1132.
[18] R. Holm, *Electrical Contacts, Theory and Applications*. Berlin, Germany: Springer-Verlag, 1976.
[19] F. W. Peek, *Dielectric Phenomena in High Voltage Engineering*. York, PA: Maple, 1929.
[20] J. G. Simmons, "Generalized formula for the electric tunnel effect between similar electrodes separated by a thin insulating film," *J. Appl. Phys.*, vol. 34, pp. 1793–1803, Jun. 1963.
[21] C. Vicente, D. Wolk, and H. L. Hartnagel, "Experimental analysis of passive intermodulation at waveguide flange bolted connections," *IEEE Trans. Microw. Theory Tech.*, vol. 55, no. 5, pp. 1018–1028, May 2007.
[22] Y. Yamamoto and N. Kuga, "PIM characteristics of resistive dummy loads," in *Proc. Asia–Pacific Microw. Conf.*, 2005, vol. 5, pp. 3133–3136.
[23] R. F. Pierret, *Advanced Semiconductor Fundamentals*. Boston, MA: Addison-Wesley, 1987.
[24] J. R. Wilkerson, K. G. Gard, A. G. Schuchinsky, and M. B. Steer, "Electro-thermal theory of intermodulation distortion in lossy microwave components," *IEEE Trans. Microw. Theory Tech.*, vol. 56, no. 12, pp. 2717–2725, Dec. 2008.
[25] R. Timsit, "Electrical Contact Resistance: Fundamental Principles," in *Electrical Contacts: Principles and Application*, P. G. Slade, Ed. Boca Raton, FL: CRC, 1999, p. 12.
[26] P. Steinmann, S. M. Jacobsen, and R. Higgins, "Controlling the TCR of thin film resistors," in *Proc. 30th Eur. Solid-State Device Res. Conf.*, 2000, pp. 452–455.
[27] J. R. Wilkerson, "Electro-thermal passive intermodulation distortion in microwave attenuators," in *Proc. 36th IEEE Eur. Microw. Conf.*, 2007, pp. 157–160.
[28] D. C. Giancoli, *Physics*, 4th ed. Englewood Cliffs, NJ: Prentice-Hall, 1995.
[29] F. Arazm and F. A. Benson, "Nonlinearities in metal contacts at microwave frequencies," *IEEE Trans. Electromagn. Compat.*, vol. EMC-22, no. 3, pp. 142–149, Aug. 1980.
[30] A. Christianson and W. J. Chappell, "Measurement of ultra low passive intermodulation with ability to separate current/voltage induced nonlinearities," in *IEEE MTT-S Int.l Microw. Symp. Dig.*, Boston, MA, 2009, pp. 1301–1304.
[31] R. W. Boyd, *Nonlinear Optics*, 3rd ed. Burlington, MA: Academic, 2008.

Justin J. Henrie (M'07) was born in Salt Lake City, UT. He received the B.S. degree in electrical and computer engineering from Brigham Young University, Provo, UT, in 2005, and is currently working toward the Ph.D. degree at Purdue University, West Lafayette, IN.

He is currently a Graduate Research Assistant with the Integrated Design of Electromagnetically-Applied Systems (IDEAS) Laboratory, Purdue University.

Andrew J. Christianson (S'05) was born in Denver, CO. He received the B.S. degree in electrical and computer engineering from Purdue University, West Lafayette, IN, in 2005, and is currently working toward the Ph.D. degree at Purdue University.

He is currently a Graduate Research Assistant with the Integrated Design of Electromagnetically-Applied Systems (IDEAS) Laboratory, Purdue University.

William J. Chappell (S'98–M'02) received the B.S.E.E., M.S.E.E., and Ph.D. degrees from The University of Michigan at Ann Arbor, in 1998, 2000, and 2002, respectively.

He is currently an Assistant Professor with the Electrical and Computer Engineering Department, Purdue University, West Lafayette, IN. He is also a member of the Birck Nanotechnology Center and the Center for Wireless Systems and Applications. His research focus concerns advanced applications of RF and microwave components. He has been involved with numerous Defense Advanced Research Projects Agency (DARPA) projects involved in advanced packaging and materials processing for microwave applications. His research sponsors have included the Homeland Security Advanced Research Projects Agency (HSARPA), Office of Naval Research (ONR), National Science Foundation (NSF), the State of Indiana, Communications-Electronics Research, Development, and Engineering Center (CERDEC), Army Research Office (ARO), as well as industry sponsors. His research group uses electromagnetic analysis, unique processing of materials, and advanced design to create novel microwave components. His specific interests are the application of very high-quality and tunable components utilizing package-scale multilayer components. He is additionally involved with high-power RF systems, packages, and applications.